Charge screening wormlike micelles affects extensional relaxation time and noodle formation

Rui Huang,[a] Daniel McDowall,[a] Henry Ng,[b] Lisa Thomson,[a] Youssra K. Al-Hilaly,[c,d] James Doutch,[e] Sam Burholt,[f] Louise C. Serpell,[c] Robert J. Poole[b] and Dave J. Adams[a,*]

a. School of Chemistry, University of Glasgow, Glasgow, G12 8QQ, U.K. Email: dave.adams@glasgow.ac.uk
b. School of Engineering, University of Liverpool, Liverpool, L69 3GH, U.K.
c. Sussex Neuroscience, School of Life Sciences, University of Sussex, Falmer, BN1 9QG, U.K.
d. Chemistry Department, College of Science, Mustansiriyah University, Baghdad, Iraq
e. ISIS Pulsed Neutron and Muon Source, Harwell Science and Innovation Campus, Didcot, OX11 0QX, UK.
f. Diamond Light Source Ltd, Harwell Science and Innovation Campus, Didcot, OX11 0QX, UK.

Supporting Information

1 Materials

1.1 1ThNapFF

1ThNapFF was synthesised as has previously been reported.[1]

2 Methods

2.1 Sample preparation

The general preparative procedure is as follows: 1ThNapFF solutions were prepared by weighing 1ThNapFF into a vial. The required volume of deionised H_2O was added followed by the required volume of a 0.5 mol/L NaCl aqueous solution. The absolute amounts of H_2O and NaCl solutions varied based on the number of NaCl equivalents were required for that sample. Following this, NaOH was added to deprotonate the 1ThNapFF. To avoid overshooting the pH and the subsequent addition of acid which would change the final NaCl concentration, an insufficient amount of NaOH (0.8 equivalents) was first added using a 2 mol/L NaOH aqueous solution. Then, the solutions were stirred overnight, and the pH adjusted up to 11.3 by the addition of either a 2 mol/L and 0.1 mol/L NaOH (the different concentrations were required depending on how large a pH change was required).

2.2 Dripping-onto-substrate

A dripping-onto-substrate (DoS) setup was created based on previous literature.[2,3] An iPhone 8 smart phone camera with a clip-on macro lens was used to record the thinning process. The clip-on macro lens enabled good quality imaging on the small area where the DoS occurs. Depending on the speed of filament breakup either the standard (30 frames per second (fps)) or slo-mo (240 fps) video functions were used. A 4 mm diameter circular glass substrate was used to pin the contact line of the sessile drop and reduce the effects of wetting. A 19-gauge flat-headed needle connected to a 10 mL syringe was used to dispense the fluid. The fluid dispensing rate was controlled by an Alaris CareFusion syringe pump. A fixed needle to substrate distance of 4 mm was used. For each fluid, 3 experiments were performed (3 droplets) and the thinning recorded.

To reduce the effects of pre-shear, the fluids were loaded into the syringe by first pulling the plunger out of the back of the fluid. The nozzle was briefly sealed with Blu-tac and the fluid poured into the back. The plunger was returned to the syringe and inverted such that the fluid flowed to plunger with the air above. Then the excess air was dispensed. It is important to remove the air to avoid bubbles and causing inaccuracy in the flow rate as the syringe pump will compress any air trapped in the pump leading to additional forces and pressures. The syringe was loaded, and the fluid dispensed at a flow rate of 5 mL/hr until the first droplet appeared at the end of the syringe. Then the fluid dispensing rate was set to 0.2 mL/hr for the measurement. For fast thinning processes this flow rate slow enough that

it does not affect the liquid bridge thinning. For slower thinning processes (>5 s), the flow must be stopped before the droplet makes contact with the substrate. Upon stopping the syringe driving, the droplet continues to grow for a few seconds, and it can be timed such that it contacts the substrate during this. The flow cannot be stopped during the thinning process because pressing the button causes vibrations throughout the setup.

Video recordings were saved as .mov files on the iPhone by default. To perform the image analysis, the videos were converted to individual frame-by-frame .tiff files. The conversion process require different software for each step as follows.

1. VLC media player (version 3.0.12) converts .mov to .mp4.[4]

An in-built tool within the VLC media software was used to convert the .mov files to .mp4 files.

2. FFmpeg (2021-04-04 build) converts .mp4 to .avi.[5]

To convert the .mp4 files to the uncompressed .tiff files, they were first converted to the .avi file format using FFmpeg using the following command line, "ffmpeg -i filename.mp4 -pix_fmt nv12 -f avi -vcodec rawvideo convertedFile.avi"

3. ImageJ (version 1.52n) converts .avi to .tiff.[6]

The .avi files were then opened in ImageJ and saved as an "Image Sequence" to a dedicated folder for that video. This resulted in a folder of .tiff files showing the process frame-by-frame.

The .tiff files were processed in MatLab (version R2021a)[7] and the 'canny edge' detection system used to extract the evolution of filament diameter with time. The filament radius was extracted at half-way along the slender filament after it had formed. The pixels/mm value was calibrated for each experiment using the outer diameter of the 19G needle as a scale bar.

The initial droplet contact and thinning is dominated by numerous factors including surface tension, viscosity and inertial forces. At later stages, a slender filament forms which subsequently thins and breaks. For the purposes of this work, the slender filament is determined to have formed when the filament height is 10 times the filament diameter.[8] This is the elastocapillary regime, previously described by Entov and Hinch (equation 1).[9]

$$(1) \quad \frac{R}{R_0} = \left(\frac{G_E R_0}{2\sigma}\right)^{\frac{1}{3}} exp\left(-\frac{t}{3\lambda_E}\right)$$

Where G_E is the elastic modulus, λ_E the extensional relaxation time, R_0 radius of the dispensing needle, R filament radius and σ the surface tension. The thinning of the slender filament is therefore fitted to an exponential decay to obtain the extensional relaxation time (λ_E). The fitting as performed in the Origin 2020 software using the "ExpDec1" equation which takes the form as shown in equation (2). ImageJ was used to analyse the frames and determine when the slender filament formed.

$$(2) \quad y = A1\ exp\left(-\frac{x}{t1}\right) + y0$$

The surface tension of these fluids was not measured meaning that the G_E cannot be calculated.

2.3 Shear and oscillatory rheology

Shear and oscillatory rheology measurements were performed on an Anton Paar Physica 101 rheometer. For the shear viscosity measurements, a 50 mm cone and plate geometry was used. The temperature was controlled and fixed at 25ºC for the measurement. The sample was poured onto the plate to reduce pre-shear before the measurement. A shear rate range of 1 – 100 s^{-1} was investigated. For each solution,

3 repeat measurements were performed and an average viscosity and standard deviation at each shear rate was calculated.

For the oscillatory frequency sweeps, a cup and vane geometry was used. A fixed oscillatory strain of 1 % was applied and a frequency range from 1 – 100 Hz studied. 3 x 2 mL solution in Sterilin vials at each NaCl concentration were prepared and measured. The 3 repeat solutions at each NaCl equivalent were measured and then averaged with errors representing the standard deviation between the repeats.

2.4 Microscopy

A Nikon Eclipse LV100 optical microscope with an Infinity 2 camera was used to collect microscope images. The microscope was used in transmission mode and images generally collected under both normal white light as well as with cross polarisers applied.

1ThNapFF solution were measured in a pool of 50 mM $CaCl_2$ (to prevent drying) on a microscope slide. The liquid was transferred to the slide by a cut Pasteur pipette. The pipette was cut to reduce shear during dispensing.

2.5 Small angle scattering

2.5.1 Small angle neutron scattering (SANS)

SANS measurements were performed at the ZOOM beamline of the ISIS pulsed neutron source at the Rutherford Appleton Laboratory (Didcot, U.K.) using a sample changer and water bath at 25 °C. The instrument was operated in pinhole collimation, with source to sample/sample to detector distance set to L1 = L2 = 4 m. This gave scattering vector (q) range of 0.004–0.722 $Å^{-1}$ where $q = 4\pi/\lambda\sin(\theta/2)$ using neutrons of wavelengths (λ) 1.75–16.5 Å by the time-of-flight technique. Data reduction was performed using MantidPlot[10] and SANS curves were fitted with SasView (versin 5.0.2)[11]

A D_2O background and the 1ThNapFF solutions were measured in UV spectrophotometer grade, 2 mm path length quartz cuvettes (from Hellma). The 2D scattering patterns were azimuthally integrated to obtain the I vs q plots. The scattering for the D_2O background was subtracted from the 1ThNapFF solutions.

2.5.2 Small angle X-ray scattering (SAXS)

Samples were loaded into 2mm OD, 1.64 mm ID diameter polycarbonate capillaries using a 1 mL syringe and 21G needle. The capillaries were sealed with a plug of polycarbonate extrusion and then epoxy resin to prevent any drying/sample loss in the evacuated sample chamber.

SAXS measurements were performed on the offline Xenocs Xeuss 3.0 instrument (Not sure you are doing this but normally you have the supplier, i.e., Xenocs, Grenoble, France), located at Diamond Light Source, Didcot. The X-ray source used for these experiments was the Gallium Metaljet D2+ (Excillum, Kista, Sweden) producing an X-ray energy of 9.24 keV. All scattering measurements were performed using a Eiger2 R 1M detector (Dectris, Switzerland) at a sample to detector distance of 1.5 m, resulting in a q range of 0.0055 to 0.29 $Å^{-1}$. Data collection was for 10 minutes for all frames.

The scattering data was processed in Dawn Science (version 2.23.0). Each frame was calibrated (using AgBeh), masked, transmission corrected, time corrected, and a background of water was subtracted. The 2D scattering patterns were then azimuthally integrated with 512 bins to obtain the 1D I vs Q plots. A logarithmic bin was performed to prevent overweighting of the fit to high Q.

2.5.3 Model fitting

The scattering data were model fitted in SasView (version 5.0.2) to structural models. For SAXS, a scattering length density (SLD) of 14.025×10^{-6} $Å^{-2}$ was used for 1ThNapFF and an SLD of 9.469×10^{-6} $Å^{-2}$ was used for the solvent (water). For SANS, an SLD of 2.377×10^{-6} $Å^{-2}$ for 1ThNapFF and 6.393×10^{-6} $Å^{-2}$ for D_2O. Cylindrical models were chosen because 1ThNapFF is known to self-assemble into worm-like micelles.[12] Cylindrical models were chosen as 1ThNapFF is known to self-assemble into worm-

like micelles. Fitting was started with the most simplistic cylinder models (fewest parameters) first, advancing to models with more parameters as required. Where more complex models were required, every model was attempted to affirm the final choice of the model that best fits the data. For all data sets, the cylinder model was combined with a power law to capture the high scattering intensity at low Q.

2.6 Transmission Electron Microscopy (TEM)

The electron microscopy grids were prepared by placing 4 μL of the sample onto formvar/carbon-coated 400-mesh copper grids (Agar Scientific). Then, the grids were washed twice with 0.22-μm-filtered milli-Q water. Uranyl acetate (2% w/v; 4 μL) was added to the grid and left for 30 seconds before blotting. The grid was then allowed to air-dry. TEM projection images were collected using a JEOL JEM1400-Plus Transmission Electron Microscope operated at 80 kV equipped with a Gatan OneView camera (4k × 4k). Images were recorded at 25 fps with drift correction using GMS3.

2.7 Hydrogel noodle formation, bridging and dry filament formation

Hydrogel noodles were prepared by injecting the 1ThNapFF solutions into a 50 mM $CaCl_2$ bath. The fluid was dispensed using a 2-20 μL pipette (Fisherbrand SureOne aerosol barrier pipette tips) while dragging the pipette tip through the trigger medium, resulting in linear noodles. Static injection generally results in curved noodles that cannot be easily bridged across gaps.

After injection, the noodles were left in the bath for 5 – 10 seconds and then lifted out using tweezers. They were picked up from one end, allowing for the whole length of the noodle to be bridge across a gap. The gel noodles were bridged across two parallel capillary tubes stuck onto a support (generally a glass dish or beaker) using ‘Blu-tac’ at a fixed distance. They were then either tested for mechanical strength or allowed to dry overnight covered by a larger dish.

For the mechanical strength tests, the excess noodle at either end was wrapped around the capillary tube to fix the noodle in position. Without this, the noodle would slide off (instead of break) upon the application of a mass, giving an inaccurate reading of the mass it could support. The mechanical strength of the wet noodles was tested by the application of 2 x 2 cm folds of tin foil. A fixed 2 x 2 cm shape was used, but different layers were used to increase the mass. A single layered 2 x 2 cm foil weighed 5 mg and a double layered one weighed 10 mg. For each NaCl equivalent, 7 noodles were prepared and loaded with weights until they broke. The largest mass that the noodle could support before breaking was recorded.

3 Results

3.1 Rheology

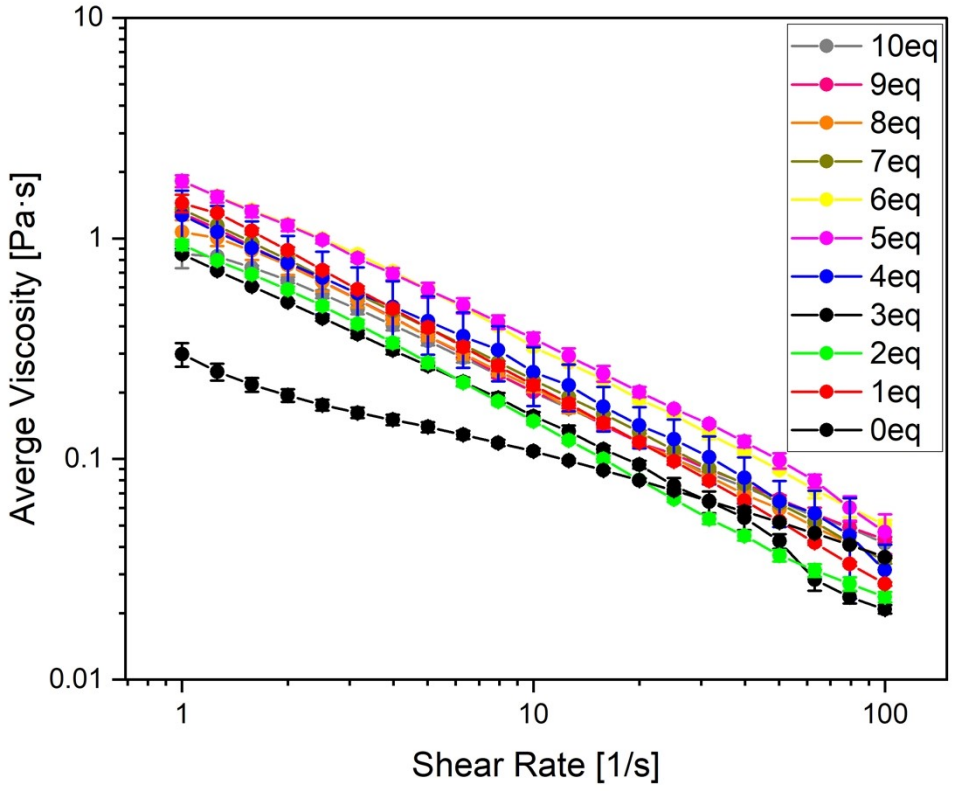

Figure S1. Shear viscosity data for 10 mg/mL 1ThNapFF solutions with different equivalents NaCl.

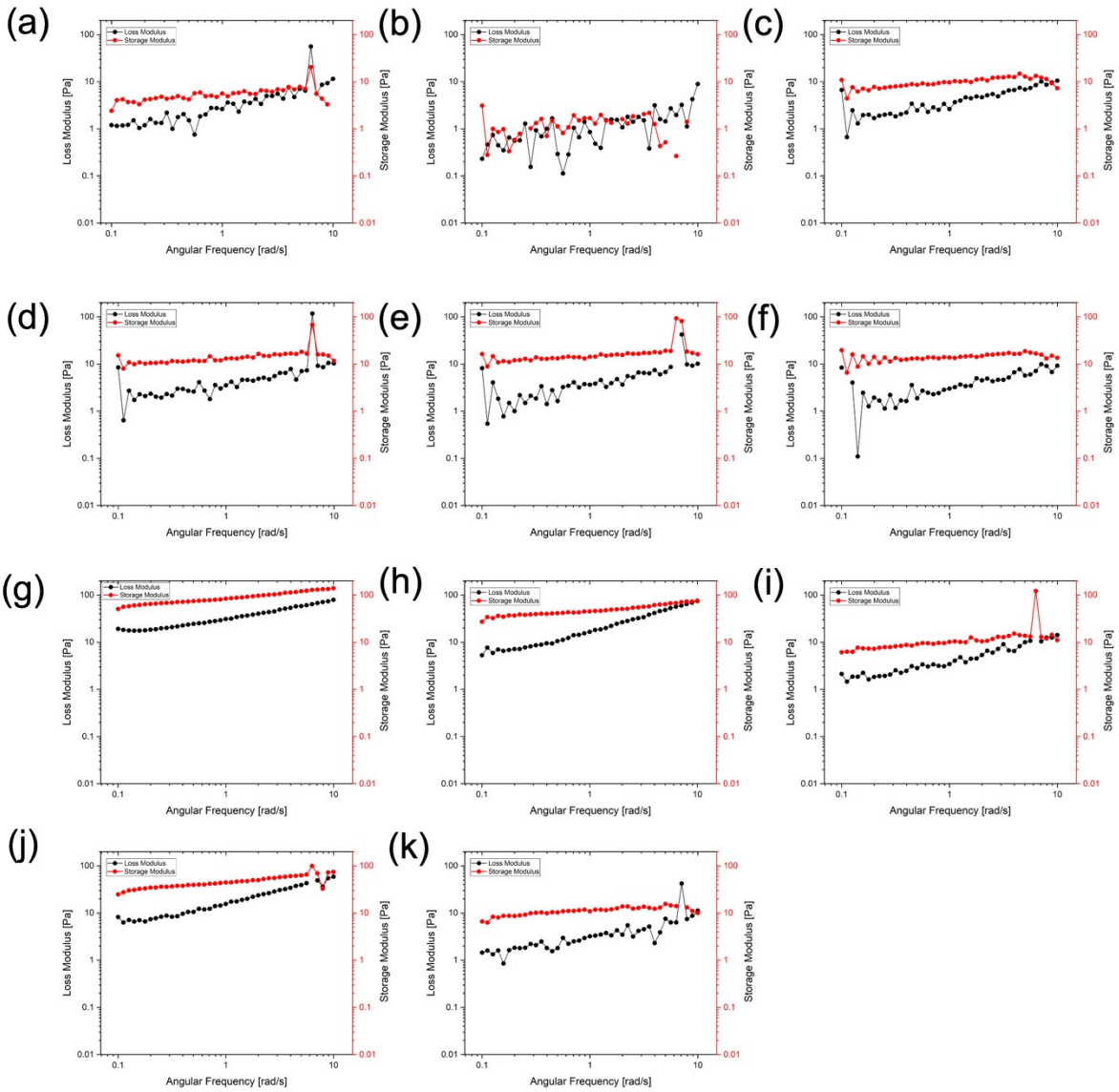

Figure S2. Oscillatory frequency sweeps data for (a) 0 eq.; (b) 1 eq.; (c) 2 eq.; (d) 3 eq.; (e) 4 eq.; (f) 5 eq.; (g) 6 eq.; (h) 7 eq.; (i) 8 eq.; (j) 9 eq. and (k) 10 eq. NaCl.

3.2 Solution cross polarised microscopy

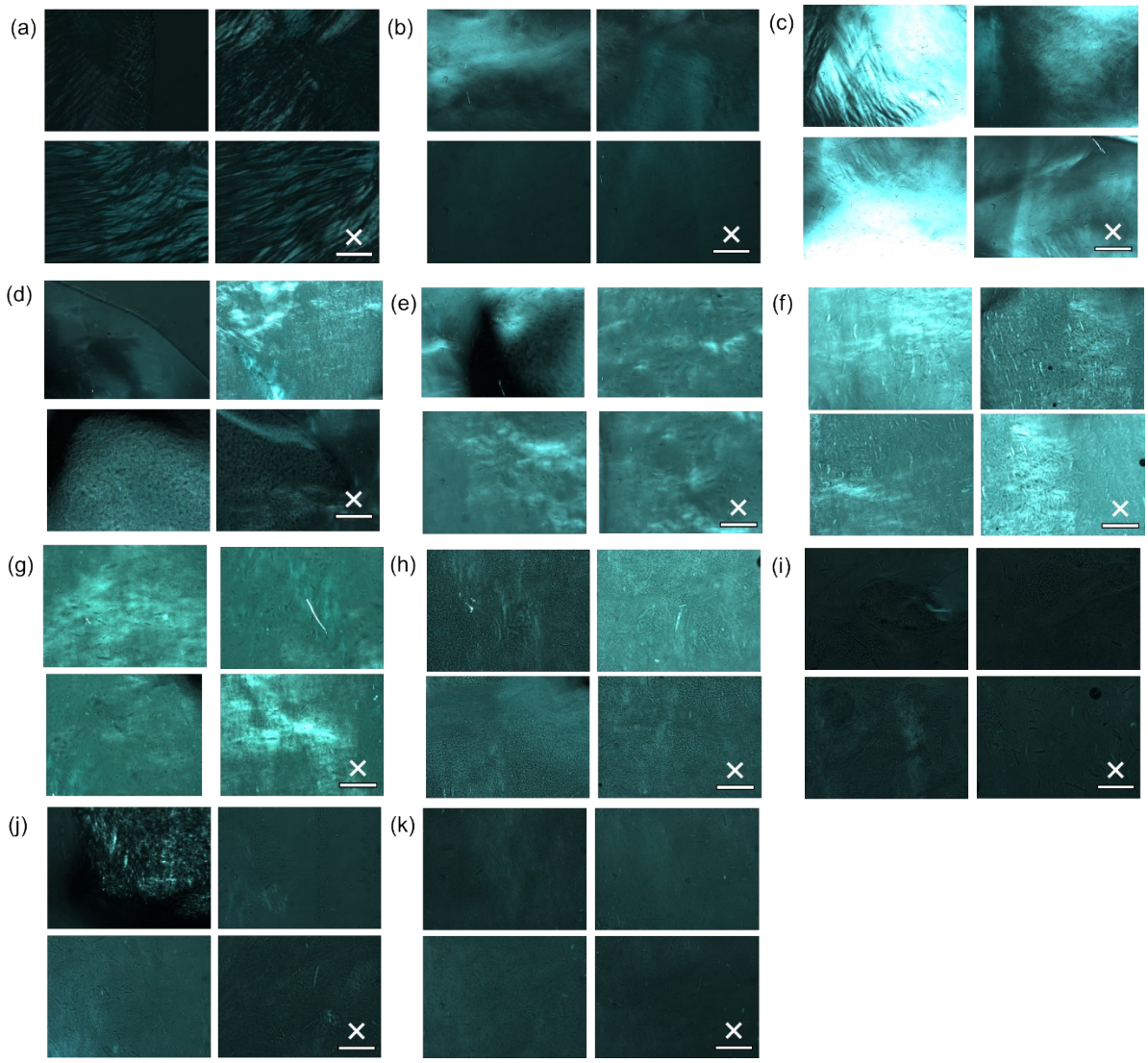

Figure S3. Cross polarised microscopy images of 1ThNapFF solutions with different NaCl equivalents (a) 0 eq; (b) 1 eq; (c) 2 eq; (d) 3 eq; (e) 4 eq; (f) 5 eq; (g) 6 eq; (h) 7 eq; (i) 8 eq; (j) 9 eq and (k) 10 eq. Scale bar represents 0.5 mm and white crosses represent polariser directions.

3.3 Dripping-onto-substrate results

As briefly covered in the main text, the solutions studied in this work showed a wide-range of behaviours during the DoS measurement. This highlights the impact of NaCl concentration because the behaviour of the liquid bridge is governed by the material properties of the fluid. The range of behaviours are described below and they meant that the limitations of the setup were found.

For some solutions, the liquid bridge broke rapidly such that an insufficient number of data points were collected by the 240 fps camera. In this instance, some information about the shape of the liquid bridge could be gained but there was not enough data to fit. For example, a small number of frames showing the formation of a slender filament, which is consistent with elastic fluid behaviour may be seen but an extensional relaxation time could not obtained. To overcome this, a higher frame rate camera (and typically higher cost!) would allow the data to be resolved. This was not deemed necessary for this study but is an important consideration.

For other solutions, the liquid bridge formed and the droplet spread over the substrate but the fluid jammed and the bridge did not break over the course of many minutes. The process is much longer than can be observed with this setup and often the fluid would dry before the liquid bridge could break. It may be an interplay of high viscosity, solid-like behaviour and surface tension but clearly the picture is complex. For example, the 6 eq. NaCl sample showed the highest shear viscosity but also showed rapid thinning in the DoS measurement.

Finally, a couple of the 9 eq. NaCl samples simply could not be fitted to the exponential decay even though the process occurred over similar timescales to the other samples that were fitted. In this case, the shape of the data was such that a good fit could not be obtained with an exponential decay.

Many of the measurements fell within timescale that could be measured by this setup. For extensional viscosity measurements, it has been highlighted in the literature that a range experimental setups are required to measure fluids possessing widely different properties.[13] As such, the setup used must be carefully considered by researchers wishing to perform such measurements.

The samples studied in this work show a degree of irreproducibility both between repeats from the same fluid and between fluids prepared in identical ways. From the literature and in measurements performed in our lab (data not shown) in which polymer solutions (such as polyacrylaminde)[3] were studied, the measurements are very reproducible. In this work, the reproducibility issues likely derive from them being wormlike micelle solutions. While they have similarities to covalent polymers, micelles can break and re-form in a manner that polymers cannot. As such, variables such as shear history (which are often hard to fully control) may lead to irreproducibility.

Many of the liquid bridge thinning processes were long (>3 seconds). Filming and processing the data for these process requires a large amount of computer power and storage space. As such, the videos were cropped prior to data processing to focus on the regions required for the exponential decay fitting. As such, the fits shown below do not show filament radii for the entire process. Instead, we show data from when a thin filament is forming.

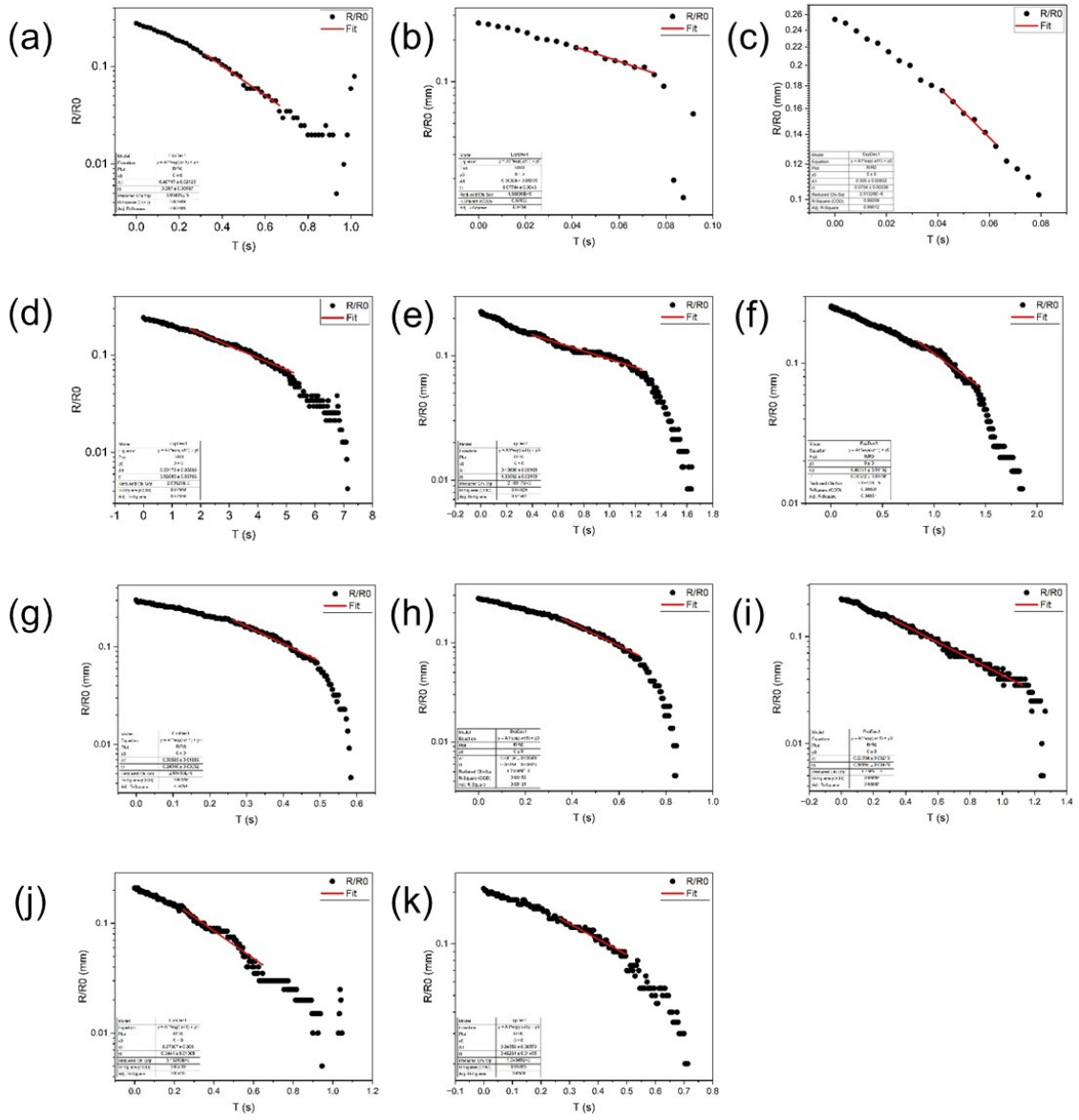

Figure S4. Exponential decay fits to aspect ratio 10 filaments for (a – c) 0 eq. NaCl; (d – k) 1 eq. NaCl. The red lines show the fits to the data.

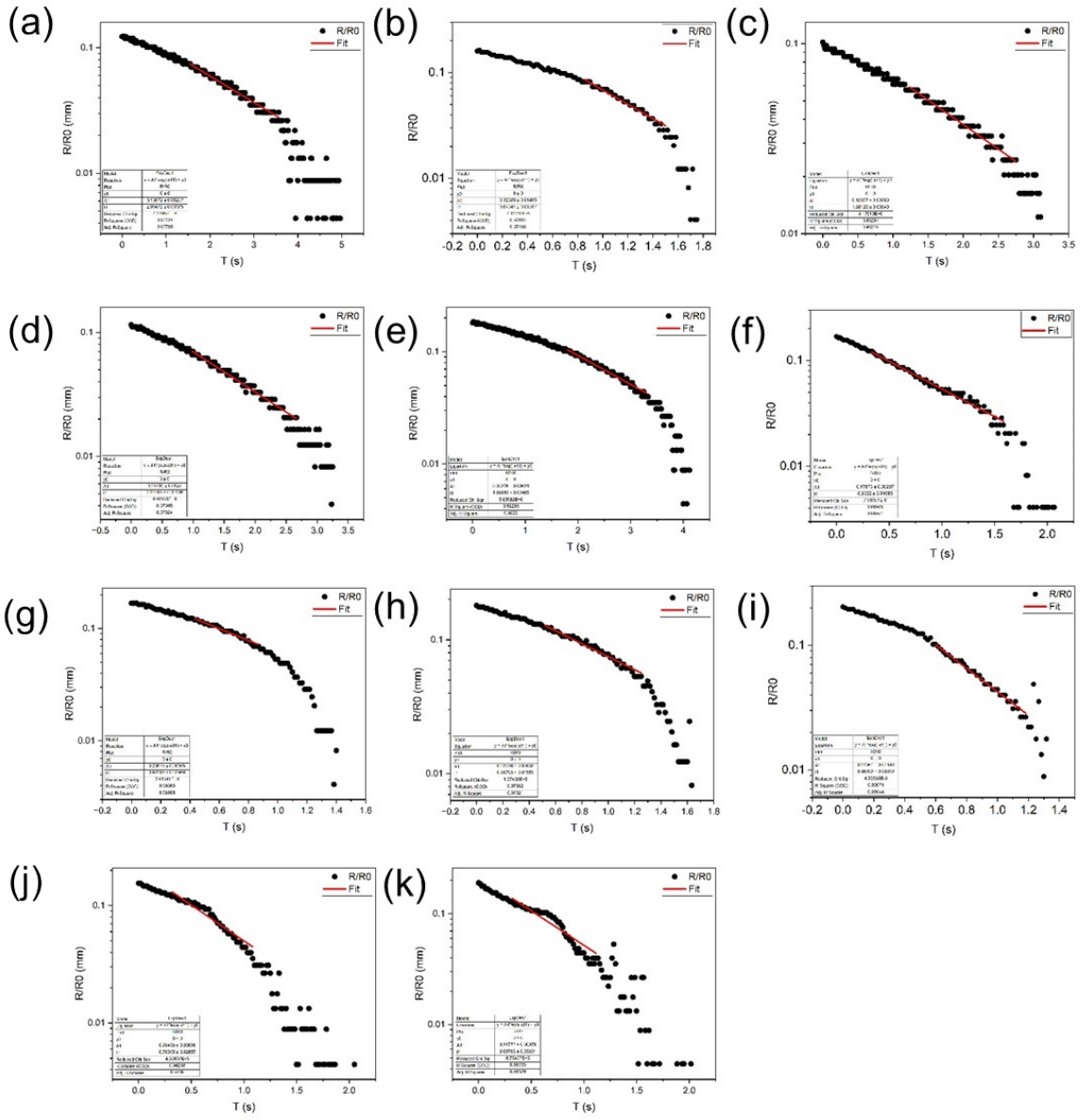

Figure S5. Exponential decay fits to aspect ratio 10 filaments for (a – d) 2 eq. NaCl; (e) 3 eq. NaCl; (f – h) 6 eq. NaCl and (i – k) 7 eq. NaCl. The red lines show the fits to the data.

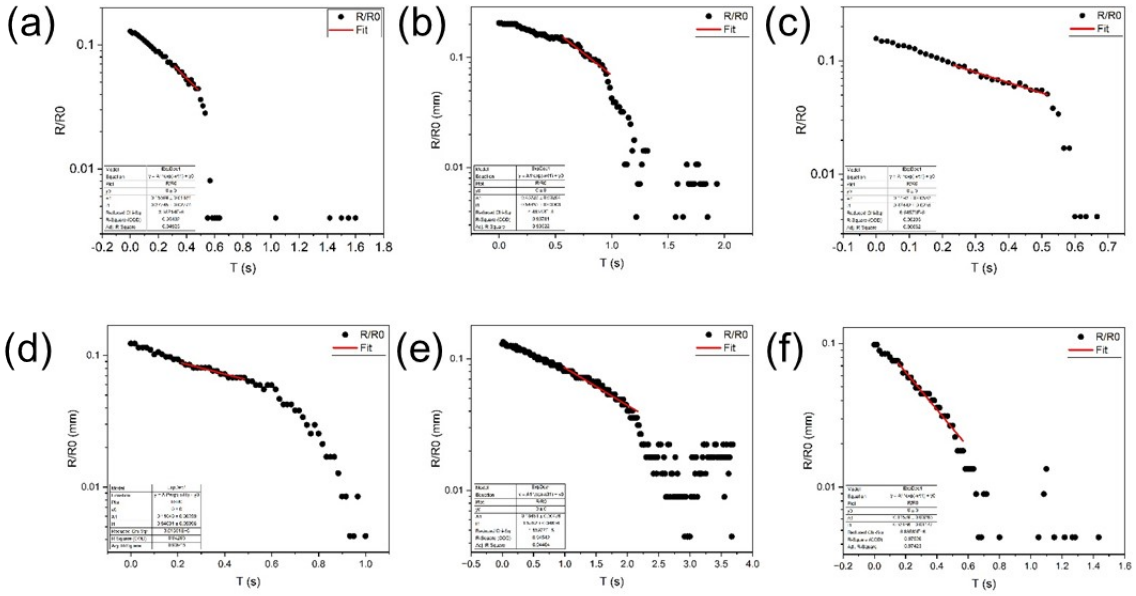

Figure S6. Exponential decay fits to aspect ratio 10 filaments for (a – b) 8 eq. NaCl and (c – f) 9 eq. NaCl. The red lines show the fits to the data.

3.3.1 Summary

Table S1. Summary of the DoS results for each NaCl equivalent. For each NaCl eq, 3 solutions were studied with 3 repeats each. Extensional relaxation times are given in seconds. Where the extensional relaxation time could not be measured, the filament either didn't break or broke to rapidly to be fitted. * indicates data that were excluded as outliers.

	0eq	**1eq**	**2eq**	**3eq**	**4eq**	**5eq**	**6eq**	**7eq**	**8eq**	**9eq**	**10eq**
R1	0.096	*1.173	0.688	Did not break	Did not break	Did not break	0.277	0.154	Did not break	0.158	Did not break
R2	Too fast	0.445	Did not break	Did not break	Did not break	Did not break	0.274	0.237	Did not break	0.313	Did not break
R3	Too fast	0.267	0.214	Did not break	Did not break	Did not break	0.299	0.232	0.126	Could not be fitted	Did not break
R4	Too fast	0.116	0.56	0.563	Did not break	Did not break	Too fast	Too fast	Did not break	Could not be fitted	Did not break
R5	Too fast	0.08	Did not break	Did not break	Did not break	Did not break	Too fast	Too fast	Did not break	Did not break	Did not break
R6	Too fast	0.128	Did not break	Did not break	Did not break	Did not break	Too fast	Too fast	Did not break	Did not break	Did not break
R7	0.026	0.19	0.447	Did not break	Did not break	Did not break	Too fast	Too fast	Did not break	0.51	Did not break
R8	0.0297	0.115	Did not break	Did not break	Did not break	Did not break	Too fast	Too fast	Did not break	0.111	Did not break
R9	Too fast	0.161	Did not break	Did not break	Did not break	Did not break	Too fast	Too fast	0.182	Did not break	Did not break

3.4 Small angle scattering

3.4.1 Small angle X-ray scattering

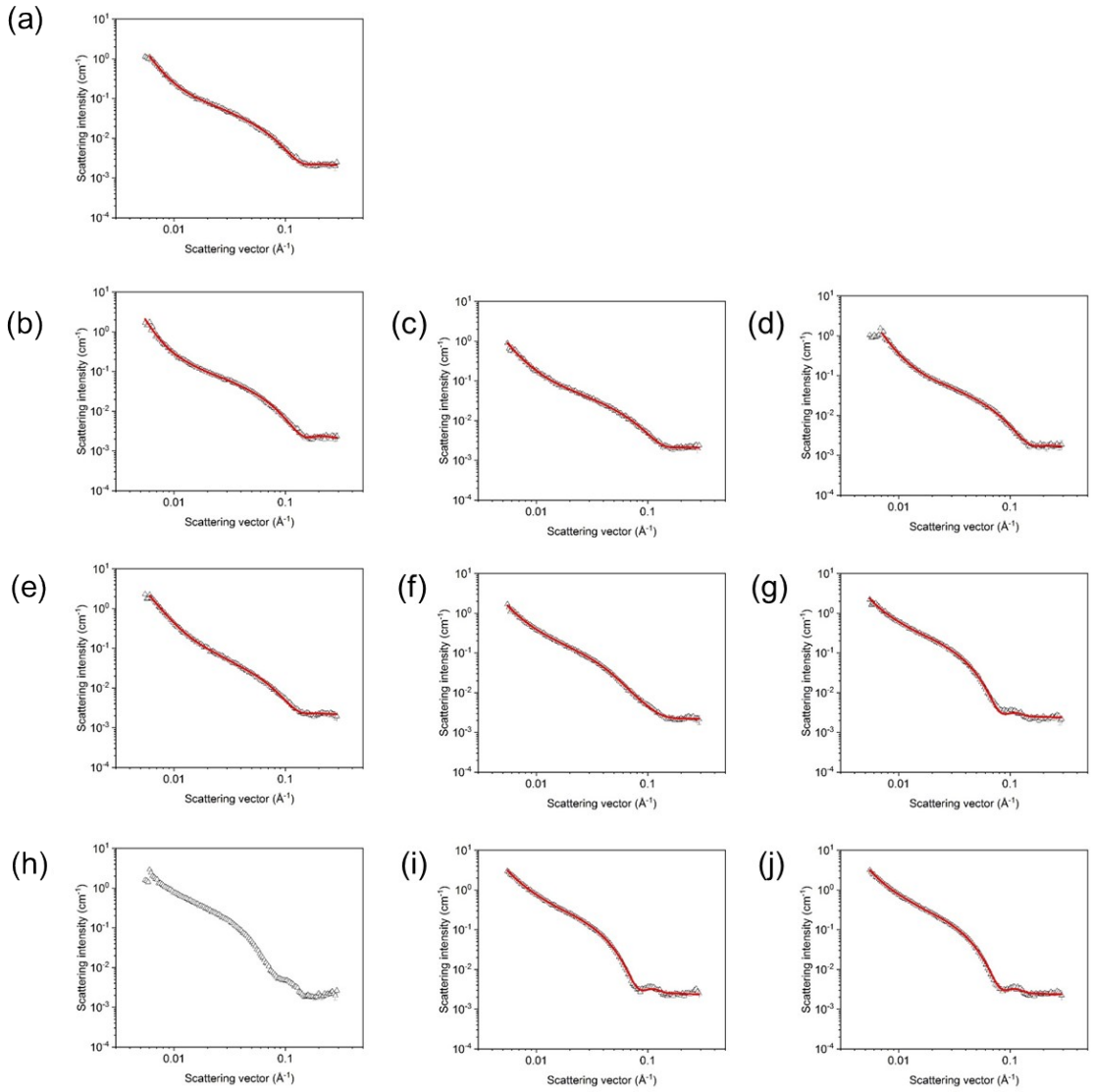

Figure S7. Small angle X-ray scattering data (hollow black triangles) and model fits (red lines) for (a) 1 eq. NaCl; (b) 2 eq. NaCl; (c) 3 eq. NaCl; (d) 4 eq. NaCl; (e) 5 eq. NaCl; (f) 6 eq. NaCl; (g) 7 eq. NaCl; (h) 8 eq. NaCl; (i) 9 eq. NaCl and (j) 10 eq. NaCl. The models used for the fits are detailed in Table S2.

Table S2. Fitting parameters for SAXS data. In the model column cyl = cylinder, PL = power law and ell cyl = elliptical cylinder. 8 eq NaCl could not be fitted.

NaCl Eq	**1**	**2**	**3**	**4**	**5**	**6**	**7**	**8**	**9**	**10**
Model	Cyl + PL	Cyl + PL	Cyl + PL	Cyl + PL	Cyl + PL	Ell Cyl + PL	Cyl + PL	-	Cyl + PL	Cyl + PL
Scale	0.00013	0.00018	0.00010	0.00015	0.00012	0.00014	0.00013	-	0.00014	0.00014
Scale error	2.1E-06	2.2E-06	2.3E-06	2.3E-06	2.0E-06	3.8E-06	6.3E-07	-	7.0E-07	7.1E-07
Background	0.0021	0.0022	0.0021	0.0017	0.0022	0.0022	0.0024	-	0.0024	0.0024
Background error	0.0001	0.0001	0.0001	0.0001	0.0001	0.0001	0.0001	-	0.0001	0.0001
Radius / Å	24.3	23.7	23.7	23.1	25.9	19.6	45.8	-	45.9	46.0
Radius error / Å	0.3	0.2	0.3	0.2	0.3	0.7	0.2	-	0.2	0.2
Axis ratio	-	-	-	-	-	2.7	-	-	-	-
Axis ratio error	-	-	-	-	-	0.1	-	-	-	-
Length / Å	556	370	504	407	192	5741	501	-	500	429
Length error / Å	90	24	91	51	13	3935	35	-	34	23
Power law scale	1.4E-10	3.9E-11	1.0E-09	2.9E-10	3.4E-08	1.7E-09	1.0E-09	-	5.6E-09	5.4E-09
Power law scale error	5.2E-11	1.4E-11	4.7E-10	7.1E-11	8.4E-09	1.0E-09	4.5E-10	-	1.8E-09	1.6E-09
Power law	4.4	4.7	3.9	4.4	3.5	3.9	4.1	-	3.8	3.8
Power law error	0.1	0.1	0.1	0.0	0.0	0.1	0.1	-	0.1	0.1
Reduced-χ2	0.94	1.88	0.72	1.74	1.17	0.58	1.29		0.98	0.84

3.4.2 Small angle neutron scattering

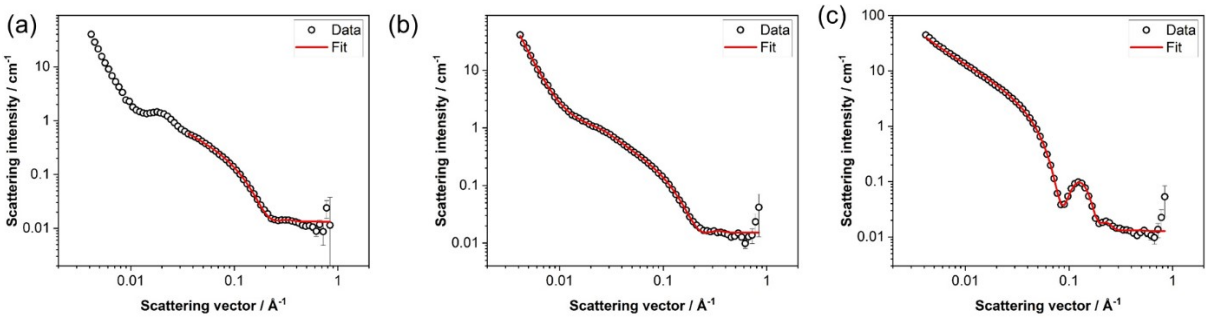

Figure S8. Small angle neutron scattering data (hollow black circles) with model fits (red lines) for (a) 0 eq. NaCl; (b) 1 eq. NaCl and (c) 10 eq. NaCl. The models used for the fits are detailed in Table S3.

A peak at Q = 0.019 $Å^{-1}$ was seen in the 0 eq. NaCl data, which corresponds to 32.4 nm.

A radial polydispersity of 0.15 was used to fit the hollow cylinder model. Without this, the fit line displayed a more well defined 'bump' at Q ~ 0.01 $Å^{-1}$, thus missing the data. The loss of well-defined peaks in the data as compared to the fit can be ascribed to either hollow cylinder polydispersity or instrumental resolution.[14]

Table S3. Fitting parameters for SANS data.

NaCl eq	**0**	**1**	**10**
Model	Cylinder	Flexible cylinder + power law	Hollow cylinder + power law
Scale	0.00584	0.006158	0.00763
Scale error	3.3E-05	3.6E-05	5.9E-05
Background	0.013	0.015	0.013
Background error	0.000	0.006	0.008
Radius / Å	15.7	14.9	17.6
Radius error / Å	0.1	0.1	0.1
Length / Å	274	182	4311
Length error / Å	29	3	59
Kuhn length / Å	-	120	-
Kuhn length error / Å	-	2	-
Thickness / Å	-	-	18.8
Thickness error / Å	-	-	0.1
Power law scale	-	7.5E-08	2.5E-05
Power law scale error	-	1.4E-08	3.5E-06
Power law	-	3.7	2.4
Power law error	-	0.0	0.0
Reduced-χ2	3.2	2.0	6.9
Comment	Fit excludes low Q where structure factor peak is	-	Polydispersity radius 0.15

3.4.3 Lateral Association

For the fitting above, an elliptical cross-section is often needed. We ascribe this to lateral association of cylindrical structures as we have shown elsewhere.[15]

In the instance of the formation of trimers and tetramers it is conceivable that they aggregate as bundles, in a planar (belt-like) fashion or a co-existence of both. In the bundle instance, it is expected that the scattering curve should be best fit to a cylinder model with a large polydispersity of cross-sectional radii. Where the bundles approximate a spherical cylinders and bundles of different radii result in

polydispersity being observed. Such a fit was attempted to the data but was unsuitable and did not capture the shape of the data at high Q as effectively as the elliptical cylinder.

For planar/belt-like structures, the axis ratio parameter from the fitting that should reflect the number of aggregated units and the formation of trimers and tetramers. In this instance, the fitting suggests the formation of a dimer is most likely. It is hard to say for certain, and this highlights a slight limitation in scattering techniques such as SAXS. Electron microscopy techniques are not without flaws also, where artefacts can be observed. We summarise our thinking in the cartoon below.

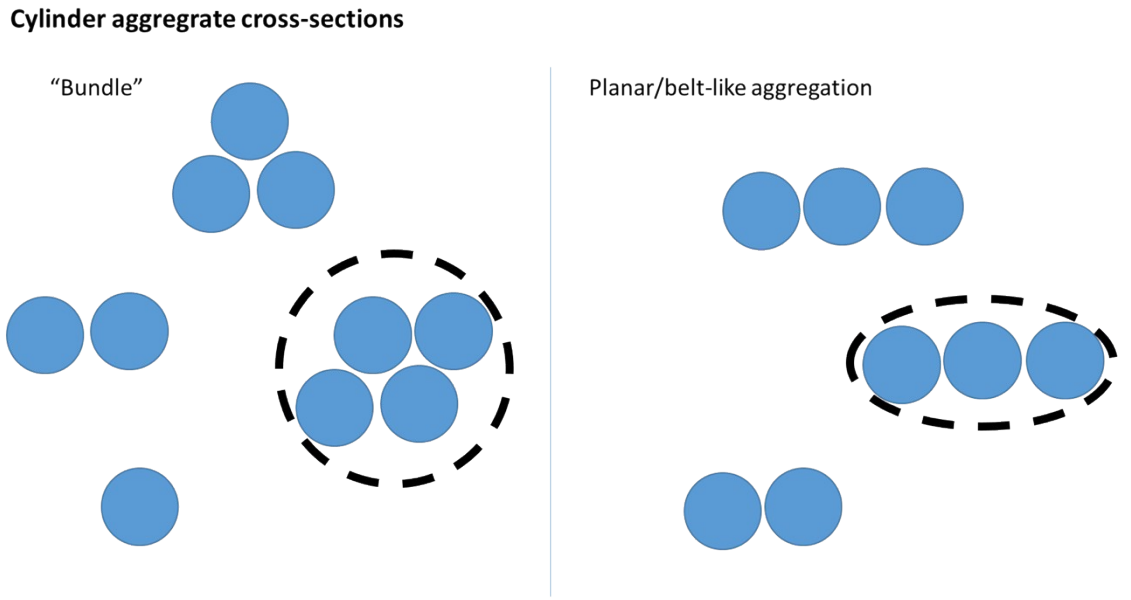

Figure S9. Cartoon showing end-on aggregation of cylindrical structures into high order aggregates could form structures with a "cylindrical" cross-section (left) or an "elliptical" cross-section (right). In both cases, the dotted lines show an example cross-section that would be detected.

3.5 TEM images

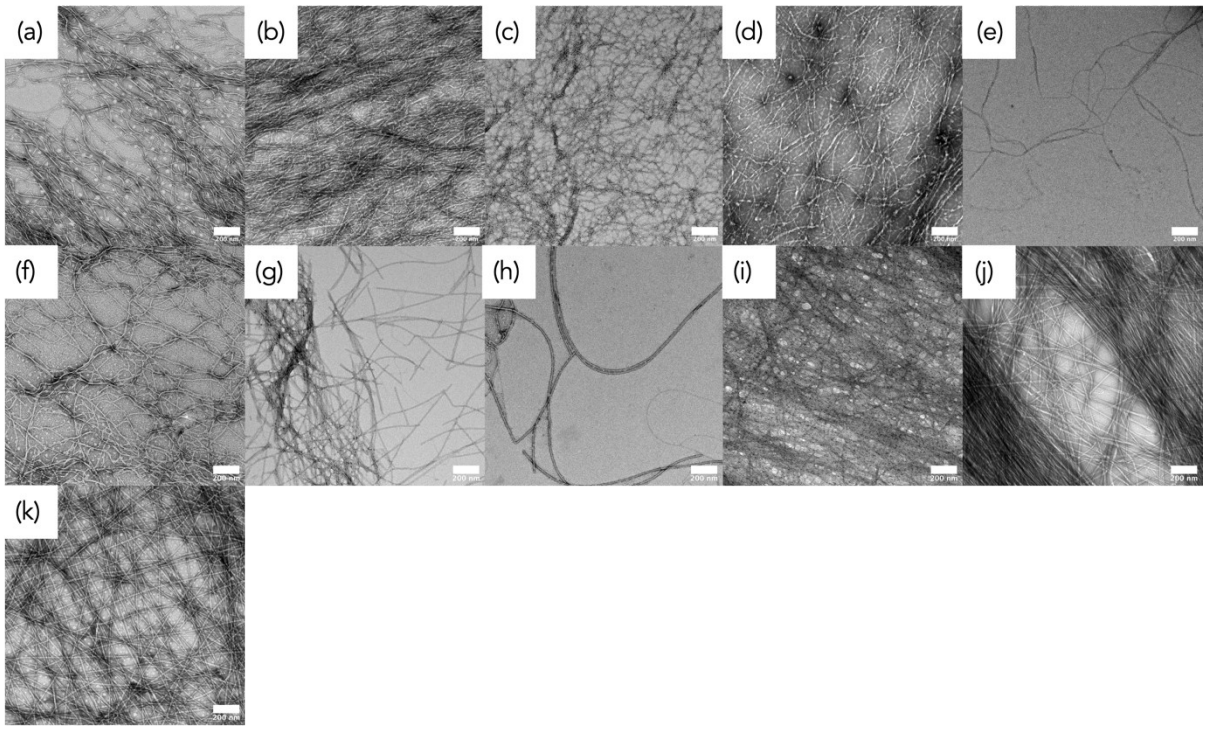

Figure S10. TEM images of (a) 0 eq. NaCl; (b) 1 eq. NaCl; (c) 2 eq. NaCl; (d) 3 eq. NaCl; (e) 4 eq. NaCl; (f) 5 eq. NaCl; (g) 6 eq. NaCl; (h) 7 eq. NaCl; (i) 8 eq. NaCl; (j) 9 eq. NaCl and (k) 10 eq. NaCl. In all cases, the scale bar represents 200 nm. Note, that there is the potential for drying artefacts in such data where it is necessary to dry the sample.

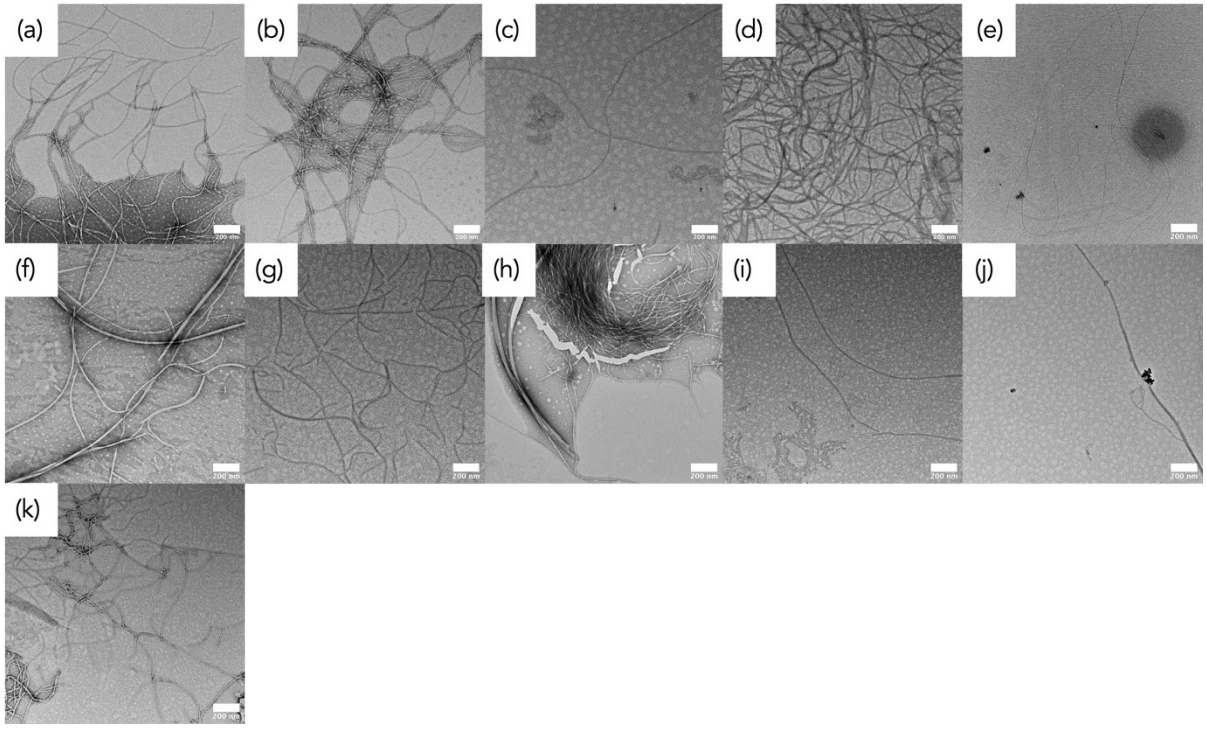

Figure S11. TEM images of gels formed by adding a solution of $CaCl_2$ to solutions[16] of (a) 0 eq. NaCl; (b) 1 eq. NaCl; (c) 2 eq. NaCl; (d) 3 eq. NaCl; (e) 4 eq. NaCl; (f) 5 eq. NaCl; (g) 6 eq. NaCl; (h)

7 eq. NaCl; (i) 8 eq. NaCl; (j) 9 eq. NaCl and (k) 10 eq. NaCl. In all cases, the scale bar represents 200 nm. In these cases, we have dried a bulk gel and so do not expect that the images capture the true 3D network, but the images do show that the network is formed from long anisotropic structures.

3.6 Noodles

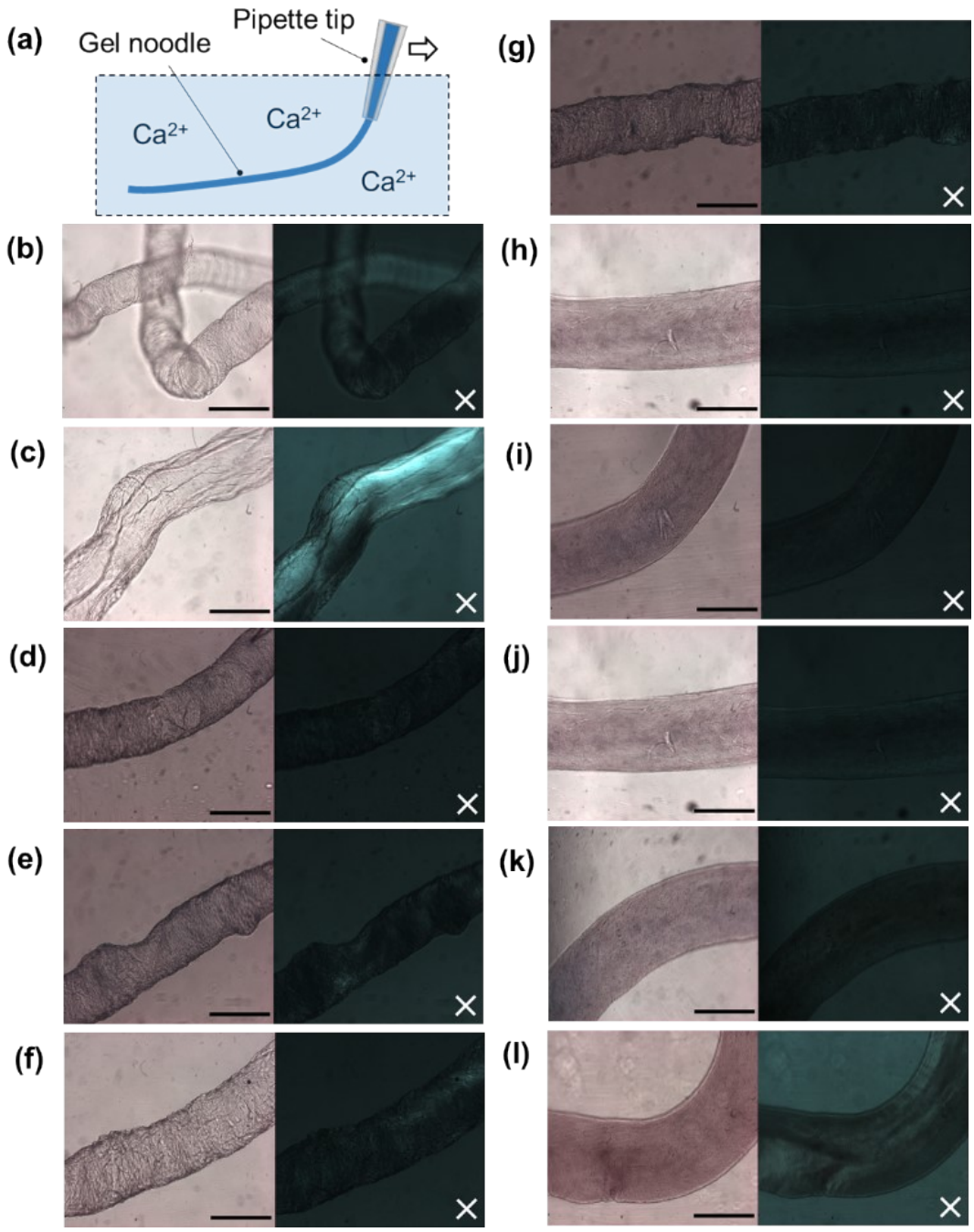

Figure 12. (a) Cartoon of noodle formation; (b)-(g) microscope images of noodles formed in a 50 mM CaCl2 trigger bath using 1ThNapFF solutions with (b) 0 eq.; (c) 1 eq.; (d) 2 eq.; (e) 3 eq.; (f) 4 eq.; (g) 5 eq.; (h) 6 eq.; (i) 7 eq.; (j) 8 eq.; (k) 9 eq. and (l) 10 eq. NaCl. Images are at 5x magnification. Noodles are imaged wet in a pool of trigger medium. Left hand images are under normal light and right hand images under cross polarised light. Scale bars represent 0.4 mm. White crosses denote the polariser direction.

3.7 Dried filaments

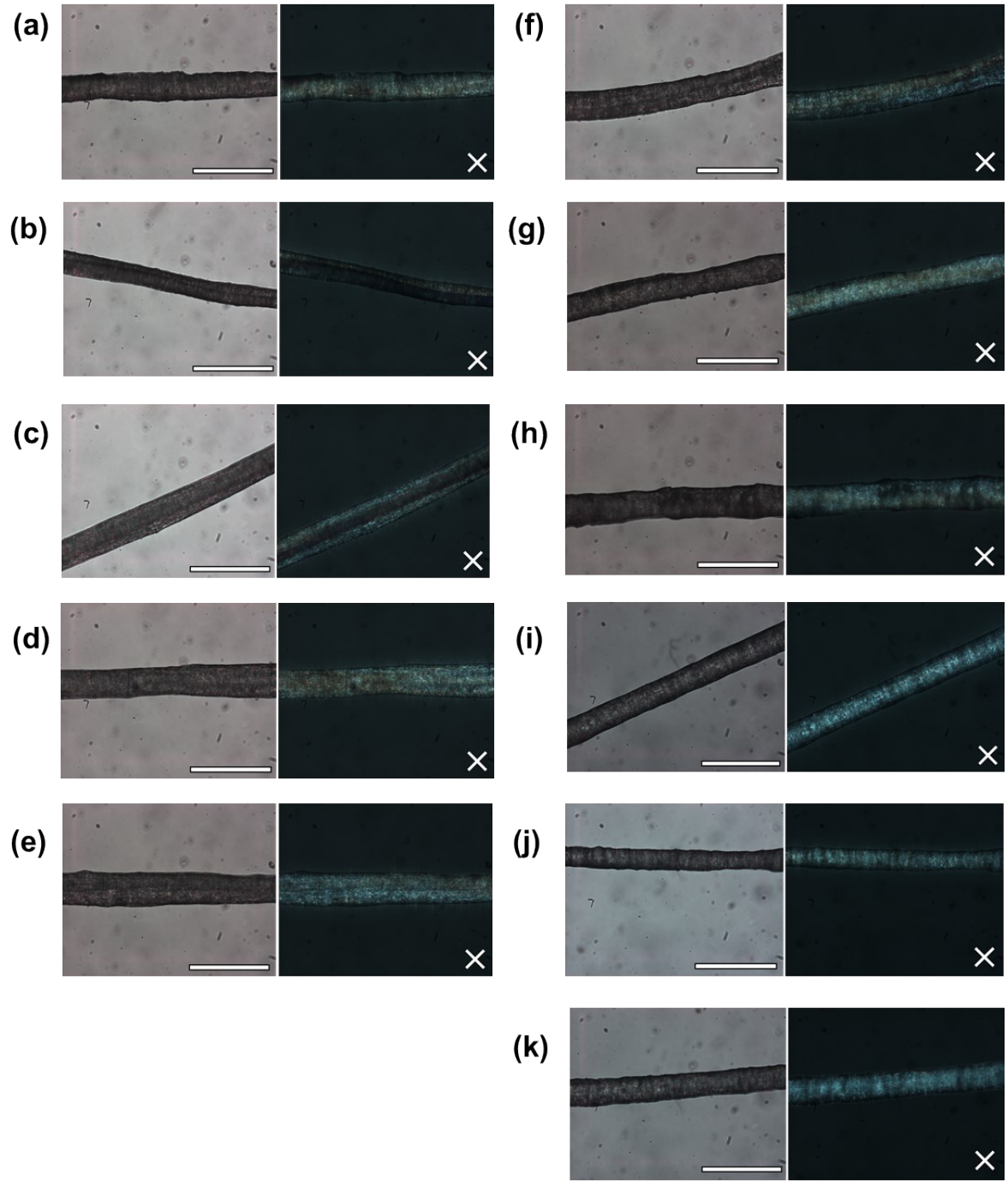

Figure S13. 20x magnification microscope images of static formed gel noodles air dried across a bridge for (a) 0 eq.; (b) 1 eq.; (c) 2 eq.; (d) 3 eq.; (e) 4 eq.; (f) 5 eq.; (g) 6 eq.; (h) 7 eq.; (i) 8 eq.; (j) 9 eq. and (k) 10 eq. NaCl. For each sample left hand images are under normal light and right hand images under cross polarised light. Scale bar represent 0.2 mm and white cross indicates polariser direction.

In many of the SEM images small crystals can be seen deposited on the surface of the structures. Energy disperse X-ray (EDX) analysis showed these crystals to comprise predominantly of Ca, Cl and Na atoms.

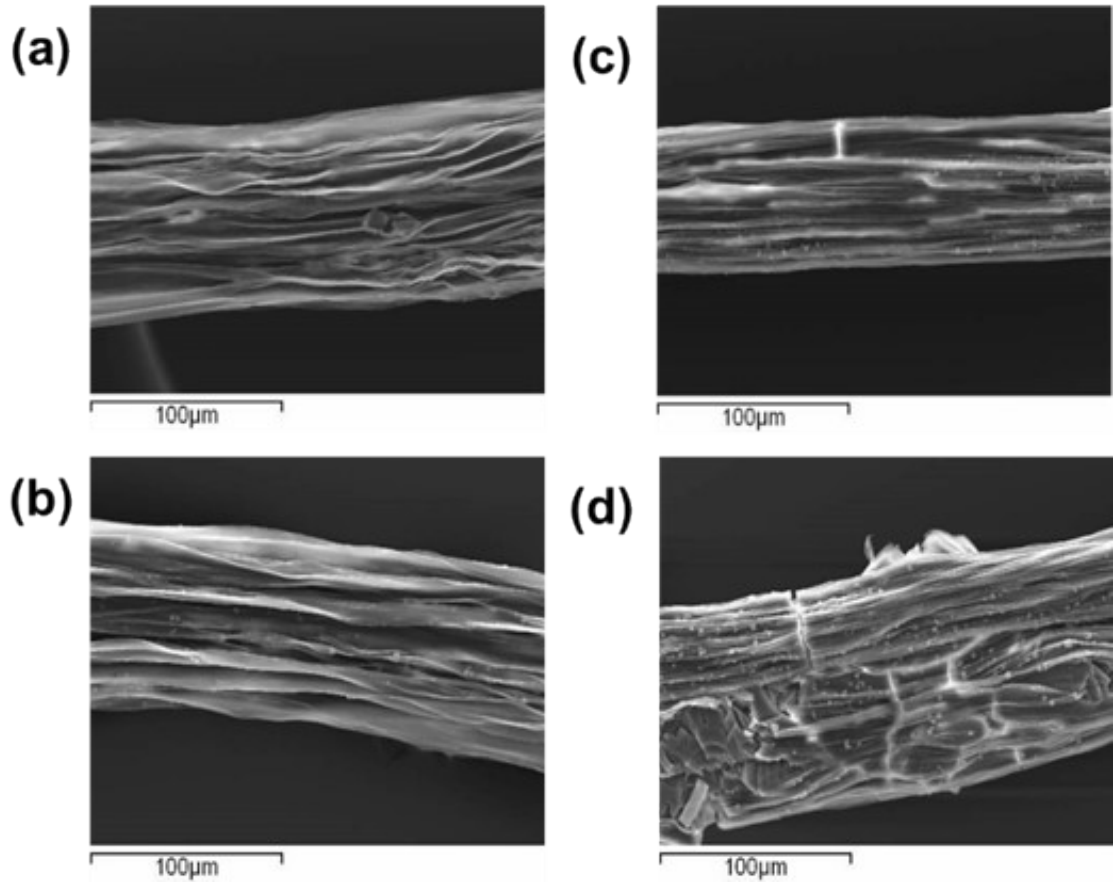

Figure S14. SEM images of static formed gel noodles air dried across a bridge for (a) 0 eq.; (b) 1 eq.; (c) 6 eq.; (d) 10 eq. NaCl.

4 References

1 M. C. Nolan, A. M. Fuentes Caparrós, B. Dietrich, M. Barrow, E. R. Cross, M. Bleuel, S. M. King and D. J. Adams, *Soft Matter*, 2017, **13**, 8426–8432.

2 J. Dinic, Y. Zhang, L. N. Jimenez and V. Sharma, *ACS Macro Lett.*, 2015, **4**, 804–808.

3 J. Dinic, L. N. Jimenez and V. Sharma, *Lab Chip*, 2017, **17**, 460–473.

4 VLC Media Player, https://www.videolan.org/vlc/, (accessed 15 April 2021).

5 FFmpeg, https://ffmpeg.org/, (accessed 16 April 2021).

6 ImageJ, https://imagej.net/Welcome, (accessed 20 October 2019).

7 MATLAB, https://uk.mathworks.com/products/matlab.html, (accessed 27 April 2021).

8 Y. Li and J. E. Sprittles, *J. Fluid Mech.*, 2016, **797**, 29–59.

9 V. M. Entov and E. J. Hinch, *J. Non-Newton. Fluid Mech.*, 1997, **72**, 31–53.

10 MantidPlot, https://www.mantidproject.org/SANS_Data_Analysis_at_ISIS.html, (accessed 31 May 2021).

11 SasView, https://www.sasview.org/, (accessed 21 September 2021).

12 D. McDowall, M. Walker, M. Vassalli, M. Cantini, N. Khunti, C. J. C. Edwards-Gayle, N. Cowieson and D. J. Adams, *Chem. Commun.*, 2021, **57**, 8782–8785.

13 V. Sharma, S. J. Haward, J. Serdy, B. Keshavarz, A. Soderlund, P. Threlfall-Holmes and G. H. McKinley, *Soft Matter*, 2015, **11**, 3251–3270.

14 F. X. Simon, T. T. T. Nguyen, N. Díaz, M. Schmutz, B. Demé, J. Jestin, J. Combet and P. J. Mésini, *Soft Matter*, 2013, **9**, 8483–8493.

15 E. R. Draper, H. Su, C. Brasnett, R. J. Poole, S. Rogers, H. Cui, A. Seddon and D. J. Adams, *Angew. Chem. Int. Ed.*, 2017, **56**, 10467–10470.

16 L. Chen, T. O. McDonald and D. J. Adams, *RSC Adv.*, 2013, **3**, 8714–8720.